A Combined MPC and PI Control Strategy for Bidirectional Interleaved Totem Pole PFC Converters in Electric Vehicle G2V and V2G Applications.

Abdellah Lassioui[1*], *Abdelaziz* Kabba[1], *Marouane* El Ancary[1], *Anwar* Hasni[1], *Yassine* El Asri[1], *Zakariae* EL Idrissi[1] and *Hassan* El Fadil[1]

[1]ISA Laboratory, National School of Applied Sciences (ENSA), Ibn Tofail University, Kénitra 14000, Morocco

Abstract. This paper presents an optimized control strategy for a bidirectional interleaved totem pole Power Factor Correction (PFC) converter, employing a combination of Model Predictive Control (MPC) and a Proportional-Integral (PI) controller. The converter's mathematical model is used to implement the MPC, which ensures a unit power factor during both Grid-to-Vehicle (G2V) and Vehicle-to-Grid (V2G) operations. Meanwhile, the PI controller regulates the DC-side voltage. It is worth noting that the MPC's design eliminates the need for a comparator to generate the Pulse Width Modulation (PWM) signal, simplifying the control architecture. The proposed control technique's effectiveness is validated through various simulation scenarios in both G2V and V2G power transfer modes, demonstrating satisfactory performance. This integrated approach provides a robust solution for efficient energy management and high-quality power conversion in bidirectional PFC converters.

1 Introduction

The rapid adoption of electric vehicles (EVs) has significantly increased the demand for efficient and reliable power conversion systems. Interleaved bidirectional AC/DC Power Factor Correction (PFC) converters are integral to this domain, offering numerous advantages. By utilizing multiple interleaved phases, these converters significantly reduce input current ripple, which minimizes the size of passive components and decreases electromagnetic interference (EMI) [1] . This design also enhances thermal management, improving system reliability and efficiency [2].

Interleaved bidirectional PFC converters are particularly valuable in EV chargers due to their bidirectional power flow capability, supporting both Grid-to-Vehicle (G2V) and Vehicle-to-Grid (V2G) operations [3]. This feature is crucial for energy storage and smart grid applications, as it allows EVs to function as distributed energy resources [4]. The totem pole topology stands out for its high efficiency and reduced component count, making it suitable

* Corresponding author: abdellah.lassioui@uit.ac.ma

for compact EV chargers [5]. Recent advancements, such as zero-voltage switching and advanced modulation techniques, have further enhanced the performance and efficiency of these converters [6]. For example, the use of LLC resonant converters in EV chargers has demonstrated improved efficiency and power density [7,8].
This paper proposes a novel control strategy that integrates Model Predictive Control (MPC) [9] with a Proportional-Integral (PI) controller for a bidirectional totem pole PFC converter in EV chargers [10,11]. This hybrid approach aims to optimize G2V and V2G operations, ensuring high efficiency and robust performance [12]. The proposed strategy eliminates the need for a comparator to generate the Pulse Width Modulation (PWM) signal, thereby simplifying the control architecture and enhancing system efficiency [13,14].

2 System overview and analysis

An interleaved bidirectional AC/DC PFC converter is a versatile and efficient system used in EV chargers. Fig. 1 illustrate a typical example. It features three "totem legs," each consisting of two high-frequency switching transistors connected to one pole of the grid voltage via a boost inductor. The use of three boost inductors reduces current ripple, enhancing efficiency and minimizing electromagnetic interference (EMI). These totem legs require advanced high-speed switching components, such as Gallium Nitride (GaN) and Silicon Carbide (SiC) devices, to handle the high switching frequencies [15].
In addition to the totem legs, the converter includes a "rectifier leg" that switches at the grid frequency [16]. The middle point of this leg connects to the opposite pole of the grid voltage, completing the circuit. Unlike the totem legs, the rectifier leg only requires silicon-based MOSFETs, which are less demanding in terms of switching speed and thermal management [15]. This combination of components optimizes the converter's performance, balancing efficiency, cost, and thermal characteristics.

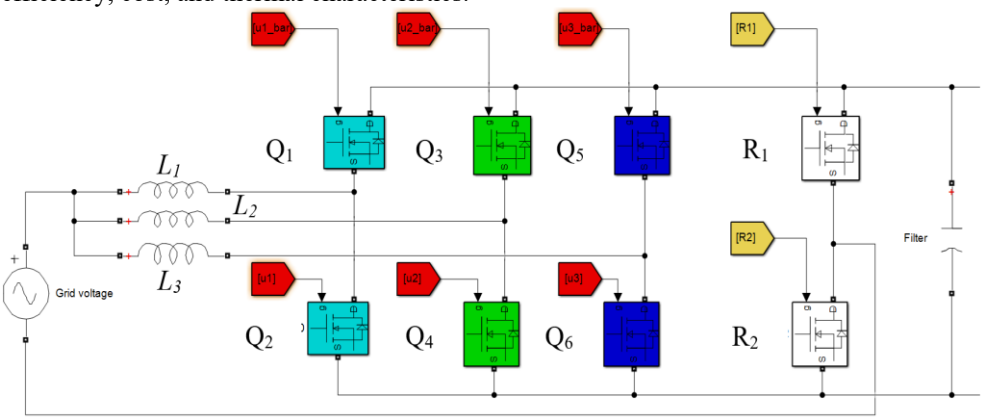

Fig. 1. Interleaved three phase bidirectional totem pole AC/DC PFC converter

To simplify the analysis, we will consider a simplified single phase AC/DC converter formed by Q_1, Q_2, R_1 and R_2 [17]. To note that the behaviour of the converter changes according to the power transfer mode (G2V and V2G) and the sign of the grid voltage [4,5]. Indeed the converter plays the role of a boost converter during G2V mode while it behaves as a buck converter during V2G mode. Table 1 summarizes all possible states of the converter's switches according to the sign of the grid voltage during G2V and V2G power transfer modes [18]. It should be noted that this analysis could be used also for the entire system shown in Fig. 1 simply by shifting the control signal applied to the other legs by 120° for leg 2 (Q_3, Q_4) and 240° for leg 3 (Q_5, Q_6) [7].

Table 1. Summary of all possible states of the converter's switches

	$V_{AC} > 0$		$V_{AC} < 0$	
G2V Mode	**Switch**	**state**	**Switch**	**state**
	- Q2	- Boost PWM	- Q1	- Boost PWM
	- Q1	- Complementary	- Q2	- Complementary
	- R2	- ON	- R1	- ON
	- R1	- OFF	- R2	- OFF
	$V_{AC} > 0$		$V_{AC} > 0$	
V2G Mode	**Switch**	**State**	**Switch**	**State**
	- Q1	- Buck PWM	- Q2	- Buck PWM
	- Q2	- complementary	- Q1	- Complementary
	- R1	- OFF	- R1	- ON
	- R2	- ON	- R2	- OFF

3 System modelling and controller design

3.1 System modelling

Equations (1) - (2) gives the mathematical model of the studied system. To note that the variable S takes 1 when the grid voltage is positive and -1 when it is negative, while D takes 1 for G2V mode and -1 for V2G mode. The variable μ_2 denotes the control signal applied to the switch Q_2. $[x_1, x_2]^T = [i_L, v_{dc}]^T$ is the state variables chosen as the inductor current i_L and the DC side voltage v_{dc} while i_0 is the current drawn by the load on the DC side.

$$\frac{dx_1}{dt} = D\frac{v_{AC}}{L} - \frac{r}{L}x_1 - D\left(\frac{1+S}{2} - \mu_2\right)\frac{x_2}{L} \tag{1}$$

$$\frac{dx_2}{dt} = -D\frac{i_0}{C_{dc}} + D\left(\frac{1+S}{2} - \mu_2\right)\frac{x_1}{C_{dc}} \tag{2}$$

3.2 Controller design

This section is devoted to the controller design task. The control objectives are twofold: i) ensuring unit power factor during both G2V and V2G modes, and ii) regulating the DC side voltage. To achieve these objectives, a combined PI and Model Predictive Control (MPC) techniques as shown in Fig.2.

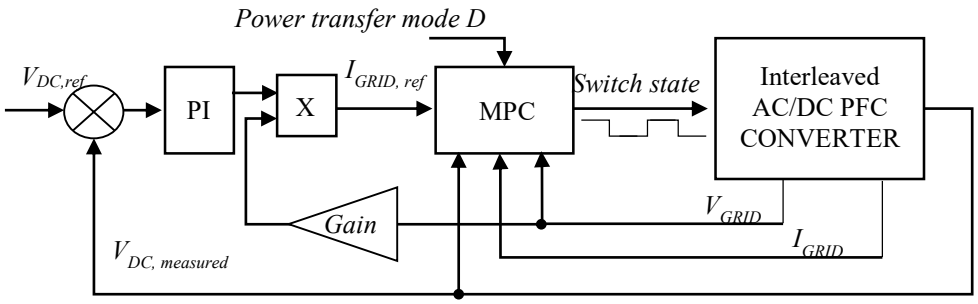

Fig. 2. General structure of the proposed control technique

The outer loop, based on PI controller ensures the regulation of the DC side voltage, while the inner loop based on the MPC technique ensures the unit power factor objective. It is worth noting that the use of MPC in the inner loop eliminates the need for a comparator to generate the PWM signal. The MPC is designed to generate the states of the switches. This approach simplifies the control architecture and enhances the system efficiency.

According to MPC technique, the optimal control state is chosen based on the predicted behavior of the system over a defined prediction horizon and the minimization criterion of the user selected cost function [19]. The prediction of the future state of the grid current is performed using the discrete form of (1) as shown in (3). Where $k=1,2...N$ is the iteration number, Ts is the sampling time and $x_1(k+1)$ is the future value of the grid current..

$$x_1(k+1)=\frac{T_S}{L}\left(Dv_{AC}-rx_1(k)-D\left(\frac{1+S}{2}-\mu_2\right)x_2(k)\right)+x_1(k) \tag{3}$$

To note that $\mu_2 = [0\ ;\ 1]$ is a vector that defines the switch state. It is worth noting that to choose the appropriate state, 0 or 1, a cost function which minimizes the current error is defined as follows:

$$Q(k+1)=\left|i_{Grid,\mathrm{Re}f}-x_1(k+1)\right| \tag{4}$$

To control the switching frequency, another cost function is defined as shown in (5) where w is a weighting factor.

$$F(k+1)=\left|\mu_2(k+1)-\mu_2(k)\right|*w \tag{5}$$

It is worth noting that the two cost functions could be combined in one function as in (6).

$$\Phi(k+1)=F(k+1)+Q(k+1)=\left|\mu_2(k+1)-\mu_2(k)\right|*w+\left|i_{Grid,\mathrm{Re}f}-x_1(k+1)\right| \tag{6}$$

That is, the optimisation problem could be as depicted in (7) [13].

$$\begin{aligned}&\mu_2(k+1)=[1;0]\arg\min_{\mu_2}(\Phi)\\&\min(\Phi(k+1))=\min(Q(k+1))+F(k+1)\end{aligned} \tag{7}$$

4 Simulation results and discussion

The effectiveness of the proposed control technique has been validated through various simulation scenarios. The obtained results are discussed in this section. As illustrated in Fig. 3, the DC side voltage initially set to 400V and later to 500V tracks the desired reference precisely without any overshoot. The simulation parameters are given in Table 2.

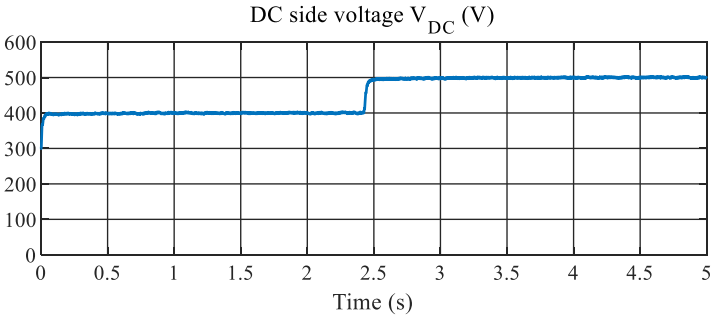

Fig. 3. DC side voltage step variations

Figure 4 shows the grid current and voltage during G2V mode, with both signals in phase, ensuring a unit power factor. Fig. 5 highlights the distribution of the main grid current among the interleaved phase currents, reducing stress on the transistors. This also improves thermal management, as the heat is distributed more evenly among phases, and enhances overall

efficiency by reducing conduction losses in the components. It also allows for higher power capacity and minimizes the size of passive components like inductors.

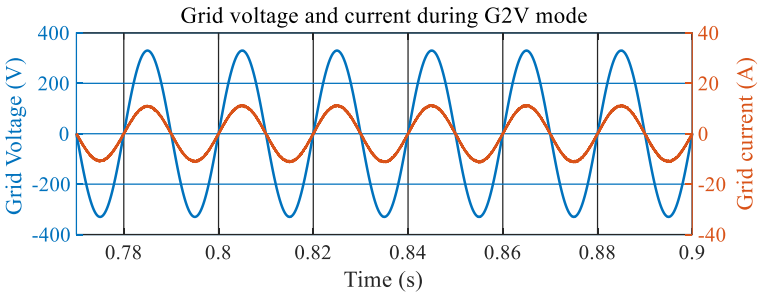

Fig. 4. Plot of the grid current and voltage during G2V mode

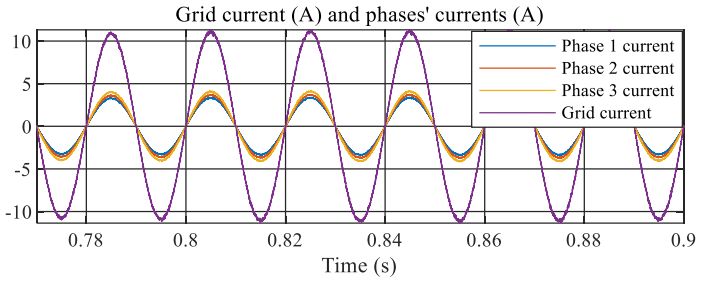

Fig. 5. Main grid current and phase's currents during G2V mode

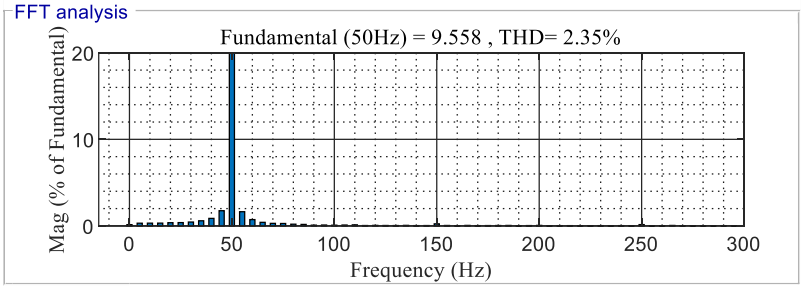

Fig. 6. Total Harmonic Distortion (THD) analysis of the grid current

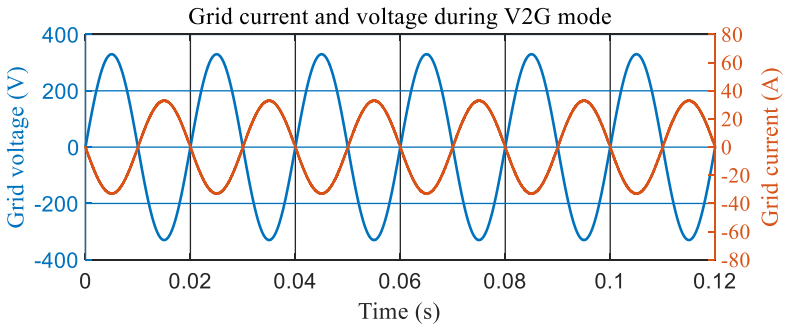

Fig. 7. Plot of the grid current and voltage during V2G power transfer mode

Figure 6 presents the total harmonic distortion (THD) analysis of the current, achieving a THD of 2.35%, which is below the recommended IEEE standard limit. Finally, Fig. 7 depicts the grid voltage and current during V2G mode, with the signals in opposite phases, ensuring a unit power factor during this mode as well. In this case, the EV acts as a power source, sending energy back to the grid. This causes the current to flow in the opposite direction compared to normal charging, resulting in the grid voltage and current being 180 degrees out of phase. This phase shift occurs because power is being supplied from the vehicle to the grid, rather than being absorbed from it as is the case in Fig 4. These results confirm the proposed strategy's capability to maintain high performance and compliance with standards in both G2V and V2G modes.

Table 2: Simulation parameters

Parameter	**Value**
Grid voltage and frequency	Vac = 230V, f = 50Hz
Inductances and internal resistances	$L1 = L2 = L3$ = 660µH, r = 1.45 mΩ
DC side filter capacitor	Cdc = 1.5mH
Switching frequency	$Fsw = 65kHz$

5 Conclusion and perspectives

In conclusion, this paper presents an efficient control strategy for an interleaved bidirectional AC/DC PFC converter, combining a PI controller and MPC. The PI controller ensures accurate DC voltage regulation, while the MPC ensures unit power factor during both G2V and V2G power transfer modes. The use of MPC optimizes the system's performance without needing a comparator for PWM generation, simplifying the control architecture. The interleaved design, featuring high-frequency components like GaN and SiC, reduces current ripple and component stress. The system achieves a low Total Harmonic Distortion (THD) of 2.35%, demonstrating compliance with IEEE standards and confirming the proposed approach's effectiveness and potential. Future work could explore further optimizations and expansions for wider grid integration and renewable energy support.

References

1. B. Singh, B. N. Singh, A. Chandra, K. Al-Haddad, A. Pandey, and D. P. Kothari, IEEE Transactions on Industrial Electronics **50**, 962 (2003)
2. S. Dharmasena, T. O. Olowu, and A. I. Sarwat, in *2019 SoutheastCon* (2019), pp. 1–5
3. A. Mallik, J. Lu, and A. Khaligh, IEEE Transactions on Vehicular Technology **67**, 8100 (2018)
4. A. Lassioui, H. El Fadil, A. M. Hamed, and E. J. Sidina, Asian Journal of Control **n/a**, (n.d.)
5. I. Bentalhik, H. El fadil, A. Lassioui, M. Koundi, Z. El idrissi, and F. Giri, IFAC-PapersOnLine **55**, 438 (2022)
6. Y. Jeong, M.-H. Park, and G.-W. Moon, IEEE Transactions on Industrial Electronics **67**, 7421 (2020)
7. J. W. M. Soares and A. A. Badin, IEEE Journal of Emerging and Selected Topics in Power Electronics **11**, 1879 (2023)
8. L. Zhou, Y. Wu, J. Honea, and Z. Wang, in *Proceedings of PCIM Europe 2015; International Exhibition and Conference for Power Electronics, Intelligent Motion, Renewable Energy and Energy Management* (2015), pp. 1–8
9. M. Schwenzer, M. Ay, T. Bergs, and D. Abel, Int J Adv Manuf Technol **117**, 1327 (2021)

10. A. Lassioui, M. El Ancary, Z. El Idrissi, H. El Fadil, K. Rachid, and A. Rachid, Processes **12**, 1264 (2024)
11. A. Lassioui, M. Elancary, H. El Fadil, Z. El Idrissi, T. Bouanou, K. Rachid, A. Rachid, and M. Koundi, in *2024 4th International Conference on Innovative Research in Applied Science, Engineering and Technology (IRASET)* (IEEE, 2024), pp. 1–6
12. A. Rachid, H. El Fadil, F. Giri, and A. Lassioui, Asian Journal of Control **22**, 1848 (2020)
13. E. Irmak and N. Güler, International Journal of Electronics **107**, 1 (2020)
14. K. Gaouzi, H. E. Fadil, Z. El-Idrissi, and A. Lassioui, International Journal of Modelling, Identification and Control **40**, 210 (2022)
15. S. Hazra, A. De, L. Cheng, J. Palmour, M. Schupbach, B. A. Hull, S. Allen, and S. Bhattacharya, IEEE Transactions on Power Electronics **31**, 4742 (2016)
16. Z. Ye, D. Zhu, and H. Yang, IEEE Power Electronics Magazine **9**, 37 (2022)
17. M. Pahlevani and P. Jain, IEEE Transactions on Power Electronics **30**, 4536 (2015)
18. F. H. El, A. Lassioui, T. Bouanou, S. Lahbabi, and H. Berbia, MA53044A1 (31 October 2022)
19. K. Gaouzi, H. El Fadil, A. Rachid, F. Z. Belhaj, and F. Giri, in *2017 International Conference on Electrical and Information Technologies (ICEIT)* (IEEE, 2017), pp. 1–5